JOURNAL OF OPTOELECTRONICS AND ADVANCED MATERIALS Vol. 10, No. 10, October 2008, p. 2631 - 2636

# Production of oxide nanoparticles by pulsed laser ablation

C. SIMA*, C. VIESPE, C. GRIGORIU, G. PRODAN[a], V. CIUPINA[a]
*National Institute for Laser, Plasma and Radiation Physics, Atomistilor 409, P.O. Box MG-36, Bucharest- Magurele, Romania.*
[a]*Ovidius University, Scientific Research Center for Micro and Nanostructures Mamaia 124, Constanta 8700, Romania.*

Oxide nanoparticles were synthesized using an advanced pulsed laser ablation system capable of reproducibly generating nanoparticles with a narrow size distribution. The production rate, size distribution, morphology, and structure of the oxide nanoparticles were investigated. Crystalline titanium, aluminum, tin, indium, nickel, zinc, and iron oxide nanoparticles were produced in an oxygen atmosphere (200 mbar) using a Nd:YAG laser (wavelength 355 nm, energy/pulse 60 mJ, repetition rate 10 pps, pulse duration 5 ns, energy density 5 J/cm$^2$). The particles were produced at an energy-related rate of 0.55-8.94 mg/J. Sizes varied between 2 and 24 nm with mean sizes in the range 3.2-10.8 nm. All oxide nanoparticles had a lognormal size distribution.

(Received June 10, 2008; accepted August 14, 2008)

*Keywords*: Metal oxide, Nanoparticles, Laser ablation, Size distribution

## 1. Introduction

There has been a great deal of recent research effort into the study and synthesis of oxide nanoparticles (NPs) due to their potential applications in the photocatalytic, environmental, biological, and solar energy fields.

Oxide nanoparticle studies have involved both chemical and physical methods. Pulsed laser ablation (PLA) is an important physical method used due to its suitability in the synthesis of high-purity functional nanocrystallites, ease of control, and adjustment of the fabrication parameters (laser wavelength, energy and power, fluence, type and pressure of ambient gas). A wide range of experimental results have been reported to date [1-30].

Production of nanopowders with a controlled narrow size distribution is a major goal in the development of future technologies. Therefore, for the PLA technique is important in ascertaining the essential factors that determine reliable NP synthesis with a controlled and reproducible size distribution [31].

One factor that plays an important role in PLA is the manner of target irradiation (irradiation pattern), particularly target ablation uniformity. In the majority of studies reported to date, the target had rotational movement or rotational and linear movement [2, 10, 15, 16, 28-30], which results in non -uniform ablation patterns over the target area.

These systems have a number of drawbacks: for example, the resulting particles are produced in a large range of sizes, or larger particles are produced with longer ablation processes.

We have developed an advanced ablation system that allows uniform irradiation over the whole target area. It consists of a computer-assisted ablation system, which maintains the same roughness during the fabrication process regardless of the number of laser pulses or the position on the target. This system takes into consideration the speed of the target, focal point area and shape, irradiation direction, etc.

This paper presents the characteristics of the NPs (oxide titanium, aluminum, tin, indium, nickel, zinc, and iron) synthesized using our PLA system. The size distribution, morphology and structure of the oxide NPs were studied by high-resolution transmission electron microscopy (HRTEM) and selected area electron diffraction (SAED).

## 2. Experimental

The experimental setup is similar to that described by Yatsui et al.[30], except that the target irradiation pattern is no longer circular but uniform over the whole target area. The targets were attached to a computer-controlled motorized X-Y translation system, driven by software that takes into account the velocity of the translation stages, the direction of movement, laser repetition rate, and the size and shape of the laser spot. Thus, the system was capable of generating nanoparticles over a narrow size range with a high degree of reproducibility.

Aluminum (99.99%), titanium (99.6%), tin (98.8%), indium (99.99%), nickel (99.5%), zinc (99.95%), and iron (99.5%) were used as targets.

A Nd:YAG laser was used, operating at a wavelength of 355 nm (third harmonic), with laser pulses of 60 mJ

energy, 10 pps pulse repetition rate, 5 ns pulse duration and 5 J/cm$^2$ fluence (density energy).

Reactive ablation was carried out under a flow of oxygen-(0.5 l/min) at a pressure of 200 mbar.

The nanopowder was collected on 100 nm pore filters.

The high resolution imaging and selected area electron diffraction were performed using Philips model CM 120 transmission electron microscope with formvar and formvar/carbon 300-mesh copper grids. Target surface roughness was measured with a Surfcom 130A/480A instrument (Tokyo-Seimitsu).

## 3. Results and discussion

During the fabrication process with the computer-assisted ablation system, the target surface roughness was 1.5±0.2 μm measured along a 4-cm path at any position on the target surface.

The large-scale manufacture of nanopowders requires cost saving methods; therefore, we investigated the nanoparticle production rate in relation to energy consumption. Table 1 summarizes the production rates for different oxides. The rates differed considerably; for example, the production rate of indium oxide was 10-fold higher than that of iron oxide. Production rate is dependent on factors as the optical and thermal properties of the target, such as the reflectivity and light absorbance of the target surface, the heat capacity, enthalpy of vaporization, boiling point, and thermal conductivity of the target [29,32]. It can be concluded from Table 1 that the low production rates (as for titanium, aluminum, nickel, and iron) were due mainly to their higher latent heat of evaporation (as compared to tin, indium, or zinc).

Table 2 shows the minimum, maximum, and mean nanoparticle sizes evaluated from HRTEM images.

*Table 1. Energy related production rate of the metallic oxides (355 nm, 200 mbar $O_2$, 60 mJ/pulse, 10 pps, 5 ns).*

| Target | Sn | In | Zn | Ni | Al | Ti | Fe |
|---|---|---|---|---|---|---|---|
| Production rate (μg/J) | 8.94 | 6.80 | 2.97 | 1.26 | 0.69 | 0.61 | 0.55 |
| Latent heat of evaporation (Jg) | 2497 | 2024 | 1748 | 6378 | 10800 | 8893 | 6095 |

*Table 2. Minimum, maximum and mean sizes of the oxide nanoparticles.*

| Target | Sn | In | Zn | Ni | Al | Ti | Fe |
|---|---|---|---|---|---|---|---|
| Minimum particle size (nm) | 3.3 | 4.4 | 4.5 | 1.5 | 1.9 | 2.2 | 2.9 |
| Maximum particle size (nm) | 14.1 | 24.2 | 22.4 | 6.0 | 12.6 | 21.3 | 18.5 |
| Mean particle size (nm) | 6.3 | 9.8 | 10.8 | 3.2 | 5.5 | 6.5 | 8.0 |

The lowest values were obtained for nickel, aluminum, and titanium oxide particles.

HRTEM images, SAED, and size distributions of the oxide nanoparticles are shown in Figures 1-7. In all cases, the size distribution was fitted with a lognormal function.

Aluminum oxide nanoparticles are shown in Figure 1; the electron diffraction pattern indicating a γ-alumina structure. The nanoparticles were approximately spherical, with diameters between 1.9 and 12.6 nm. To assess the importance of target irradiation uniformity in the production of small particles with a narrow size range, we compared these results with those of our previous study[30] (γ-$Al_2O_3$, circular irradiation pattern, 1064 nm, 16 J/cm$^2$). For the circular irradiation pattern, the maximum size of the nanoparticles was 32 nm; in the present case (uniform irradiation, 355 nm, 5 J/cm$^2$), the maximum size decreased to 12.6 nm. Comparison of the two cases indicated that the effects of wavelength and fluence were significant, but that target irradiation uniformity was the most important factor, demonstrating the advantages of an ablation system capable of maintaining a similarly low surface roughness over the whole ablated area. In studies where alumina nanoparticles were produced in liquids or with femtosecond lasers [1, 2], the best results showed wider distributions of 45-50 nm, demonstrating the importance of irradiation uniformity.

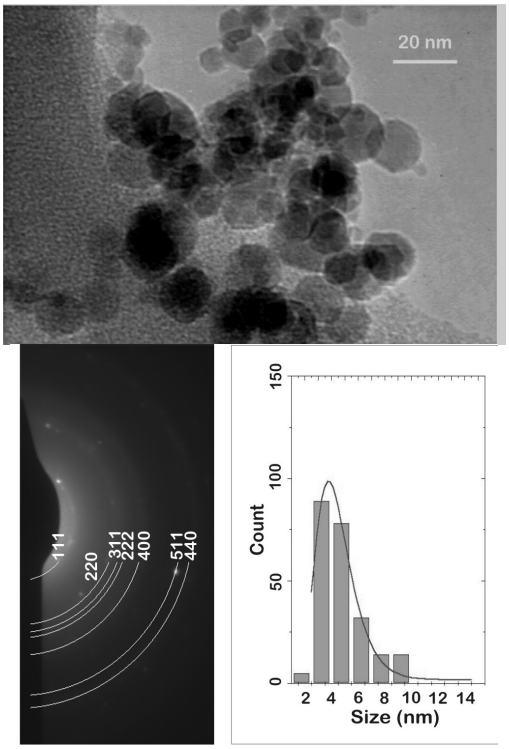


*Fig. 1. HRTEM image, SAED and size distribution of the aluminum oxide nanoparticles.*

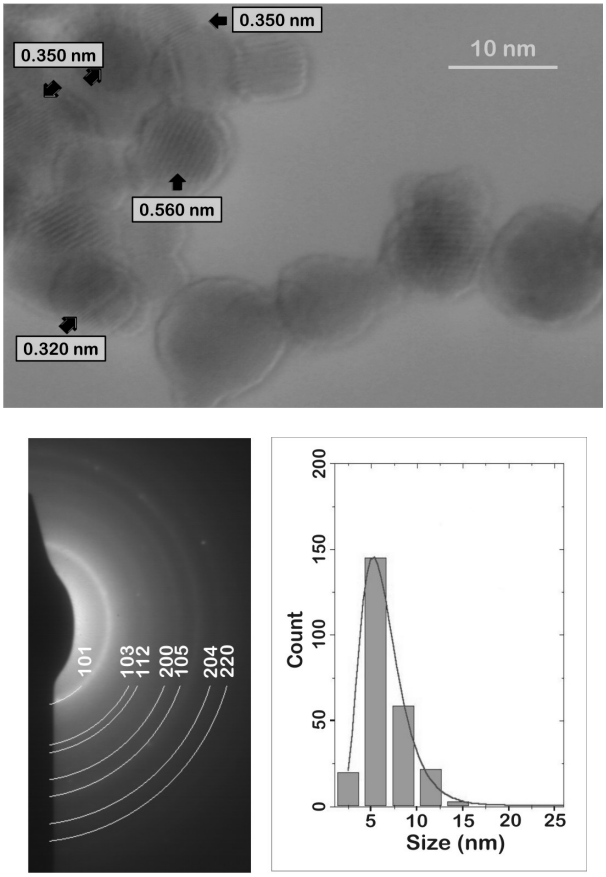


*Fig. 2. HRTEM image, SAED and size distribution of the titanium oxide nanoparticles.*

Fig. 2 shows HRTEM images of complete crystalline titanium oxide nanoparticles. The oxide titanium nanoparticles were almost spherical in shape. From the diffraction pattern (Figure 2b), the $TiO_2$ structure could be identified as tetragonal. The predominant phase was anatase with a very small amount of rutile. Figure 2a shows interference fringes associated with (101) 0.350 nm planes. The 0.320 nm lines can be indexed as (110) planes, specific for the rutile phase of $TiO_2$. The 0.560 nm lines were Moiré fringes, which appeared at the superposition of two nanocrystals.

In studies of titania fabrication by PLA[9, 16, 23-25, 27-29], the anatase phase was predominant in some cases [23,25], while the rutile was dominant in others [28, 29]. Liang et al.[23] studied the phase transformation in heat treated nanoparticles and concluded that, although the

rutile phase is stable at the macroscopic level, the anatase phase is more stable if the size of the nanoparticles is < 14 nm. This confirmed our observations where the majority of nanoparticles were less than 14 nm.

Figure 3 shows a reconstructed image based on Fourier transform, revealing dislocation in a $TiO_2$ nanocrystal. Such crystal imperfections can be explained by fast cooling in the background oxygen [24].

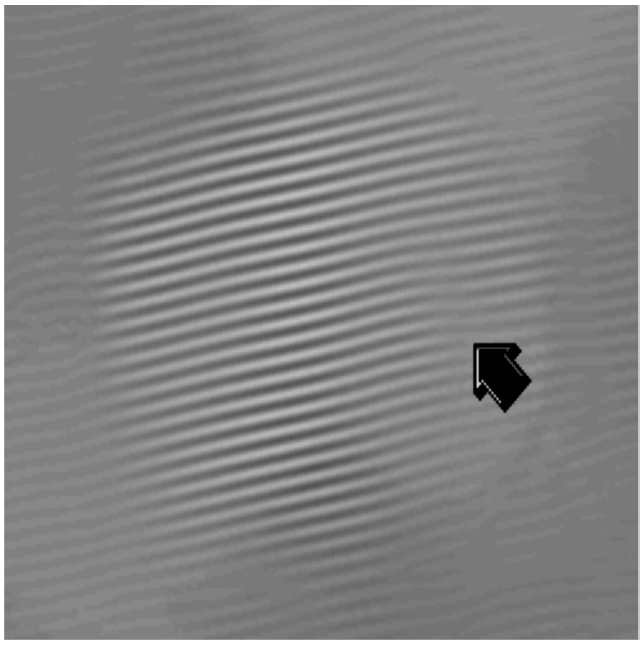

*Fig.3. Dislocation in a $TiO_2$ nanocrystal.*

Tin oxide nanoparticles (Figure 4) had a spherical shape and a mean diameter of 6.3 nm; most were around 5 nm in diameter. A representation in the Fourier space is shown in the upper right of Figure 4a, which allowed indexing of spots and determination of crystal orientation. Interference fringes specific to crystalline planes with an interplanar distance of 0.330 nm (110) were observed.

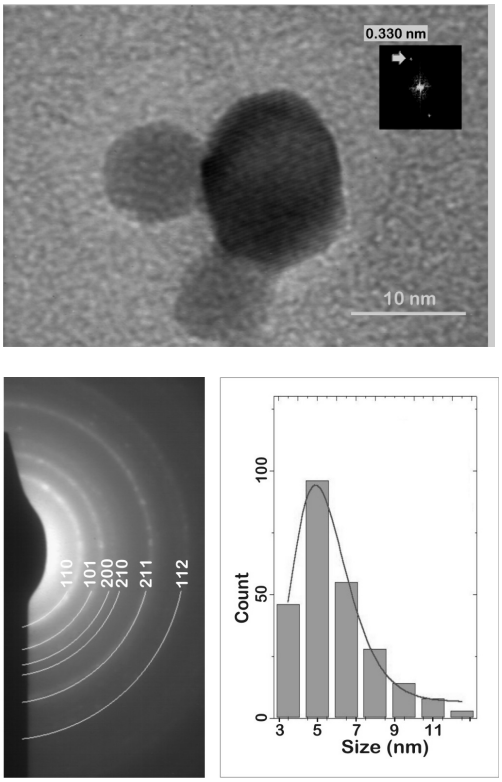


*Fig. 4. HRTEM image, SAED and size distribution of the tin oxide nanoparticles.*

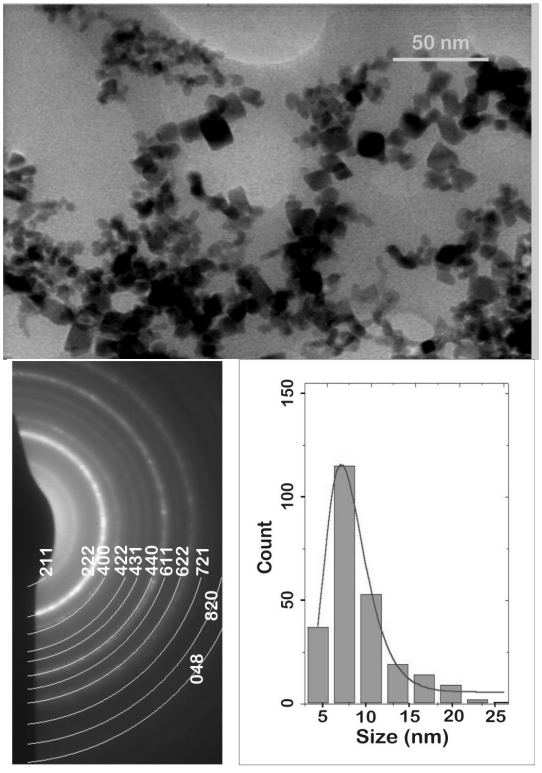


*Fig. 5. HRTEM image, SAED and size distribution of the indium oxide nanoparticles.*

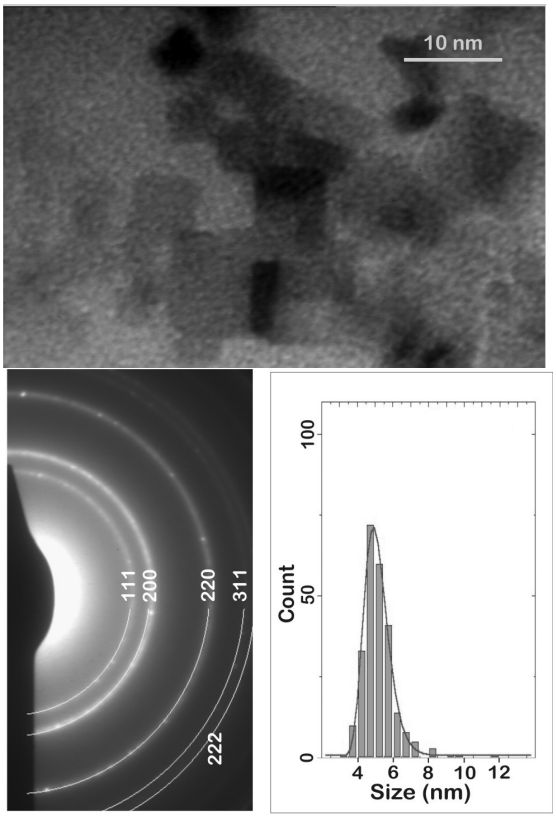


*Fig. 6. HRTEM image, SAED and size distribution of the nickel oxide nanoparticles.*

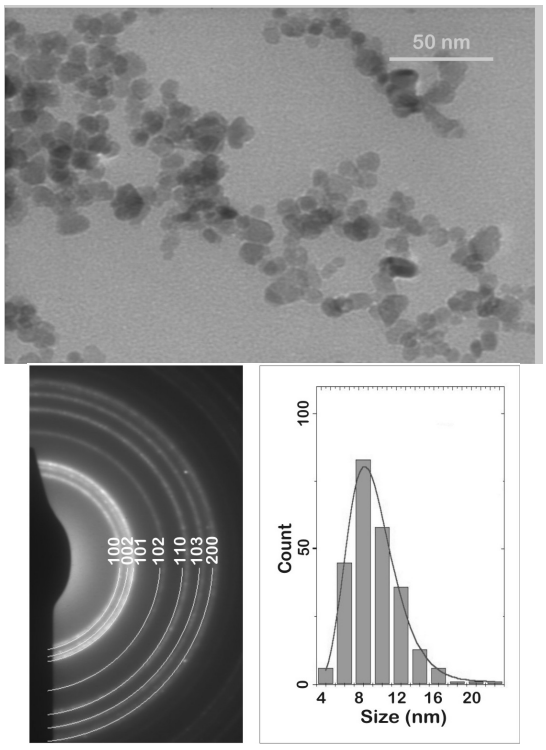


*Fig. 7. HRTEM image, SAED and size distribution of the zinc oxide nanoparticles.*

From the electron diffraction pattern, the tin oxide nanoparticle structure was identified as tetragonal according to ASTM 41-1445.

Indium oxide nanoparticles had a rectangular shape (Fig. 5a), with a mean size of 9.8 nm, the maximum being approximately 7 nm. From electron diffraction measurements, a cubic indium oxide structure was identified (according to ASTM 76-0152), with a = 1.012 nm.

Fig. 6 shows nickel oxide nanoparticles with a cubic shape and maximum size of 5 nm. Zinc oxide nanopowder is shown in Figure 7. The particles were relatively spherical (shape factor 0.86), with a maximum size distribution of ~8 nm.

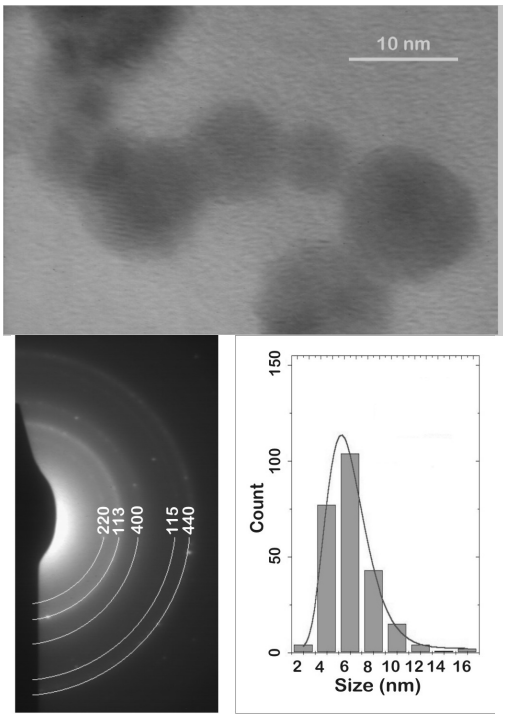


*Fig. 8. HRTEM image, SAED and size distribution of the iron oxide (magnetite) nanoparticles.*

From electron diffraction patterns, a hexagonal structure was identified with lattice constants a = 0.324 nm and c = 0.520 nm.

Iron oxide (magnetite) nanoparticles are presented in Figure 8. The particles were relatively spherical, and most were ~6.5 nm in diameter. A cubic structure was identified via SAED, with lattice constant a = 0.839 nm (WWW-MINCRYST, magnetite-2701).

## 4. Conclusions

We successfully prepared titanium, aluminum, tin, indium, nickel, zinc, and iron oxide nanoparticles using an advanced pulsed laser ablation method, which permitted uniform target irradiation, and, consequently, reproducible NP production.

NPs, with sizes ranging 2-24 nm and lognormal size distribution, were produced at an energy-related production rate of 0.55-8.94 mg/J.

The system yielded spherical γ-alumina (5.5 nm mean size), spherical titanium oxide nanoparticles (anatase predominant phase, 6.5 nm mean size), rectangular indium oxide (cubic structure, 9.8 nm), spherical tin oxide (tetragonal structure, 6.3 nm mean size), rectangular nickel oxide (cubic structure, 3.2 nm mean size), spherical zinc oxide (hexagonal structure, 10.8 nm mean size), and spherical magnetite (cubic structure, 8 nm mean size).

## References

[1] P. Moreno, C. Mendez, G. Torchia, D. Delgado, J. Vasquez, I. Arias and L. Roso, J. Nanosci. Nanotechnol., **6**, 1961, (2006)
[2] P. Reissaus, T. Waldemarsson, J. Blum, D. Clement, I. Llamas, H. Mutschke and F. Giovane, J. Nanopart. Res., **8**, 693 (2006)
[3] T. Sasaki, Y. Shimizu, N. Koshizaki, J. Photochem. Photobiol. A, **182**, 335 (2006)
[4] M. Tsai, S. Chen, R. Shen and P. Shen, J. Appl. Phys., **99**, 054302 (2006)
[5] S. Senkan, M. Kahn, S. Duan, A. Ly and C. Leidholm, Catal. Today, **117**, 291 (2006)
[6] Z. Haibo, C. Weiping, L. Yue, H. Jinlian and L. Peisheng, J. Phys. Chem. B, **109**, 18260 (2005)
[7] T. Sasaki, L. Changhao, H. Usui, Y. Shimizu and N. Koshizaki, MRS Proc., **847**, 243 (2005)
[8] H. Usui, Y. Shimizu, T. Sasaki, and N. Koshizaki, J. Phys. Chem., **109**, 120 (2005)
[9] C. Liang, Y. Shimizu, T. Sasaki and N. Koshizaki, Appl. Phys. A Mater., **80**, 819 (2005)
[10] L. Zbroniec, T. Sasaki and N. Koshizaki, J. Ceram. Process., **6**, 134 (2005)
[11] T. Okada, K. Kawashima, N. Ueda, and Y. Nakata, Proc. SPIE, 5713, 576 (2005)
[12] A. Pereira, A. Cros, P. Delaporte, T. Itina, M. Sentis, W. Marine, A. Thomann and C. Boulmer, Proc. SPIE, **6263**, Q2630 (2005)
[13] T. Sasaki, Y. Shimizu and N. Koshizaki, Rev. Laser Eng. **1**,18 (2005)
[14] T. Tsuji, T. Kawamura, J. Yamaki and M. Tsuji, Appl. Surf. Sci., 243, 214 (2005)
[15] X. Zeng, Z. Wang, Y. Liu and M. Ji, Appl. Phys. A Mater., **80**, 581 (2005)
[16] T. Sasaki, C. Liang, W. Nichols, Y. Shimizu and N. Koshizaki, Appl. Phys. A- Mater. , **79**, 1489 (2004)
[17] T. Okada, A. Hartanto, Y. Nakata, Proc. SPIE, **5339**, 357 (2004)
[18] T. Seto, K. Koga, H. Akinaga, F. Takano, K. Sakiyama, M. Hirasawa T. Orii, Appl. Phys. A-Mater., 79, 1104)
[19] K. Sakiyama, K. Koga, T. Seto, M. Hirasawa and T. Orii, J. Phys. Chem. B, **108**, 523 (2004)
[20] S. Orlando, A. Paladini, A. Santagata, V. Marotta, G. Parisi, M. Satta, D. Scuderi, D. Catone, A. Giardini and A. Mele, Int. J. Photoenergy, **6**, 23 (2004)

[21] H. Lam, M. Hong, S. Yuan, T. Chong, Appl. Phys. A -Mater **79**, 2099 (2004)
[22] T. Okada, K. Kawashima, Proc. SPIE **5662**, 420 (2004).
[23] C. Liang, Y. Shimizu, T. Sasaki, N. Koshizaki, J. Mater. Res. **5**, 1551 (2004).
[24] M. Tsai, S. Chen and P. Shen, Nanoletters **4**, 1197 (2004).
[25] A. Iwabuchi, C. Choo, K. Tanaka, J. Phys. Chem. B, **108**, 10863 (2004).
[26] T. Okada, N. Kawakami, A. Hartanto, Y. Nakata, Proc. SPIE **4977**, 362 (2003).
[27] N. Aya, S. Kano, T. Seto, M. Hirasawa, T. Orii, K. Sakiyama, H. Shimura, Proc. SPIE **4830**, 228, (2003).
[28] M. Matsubara, T. Yamaki, H. Itoh, H. Abe, K. Asai, Jpn. J. Appl. Phys. **42**, L479 (2003).
[29] M. Ullmann, S. K. Friedlander, A. Schmidt-Ott, J. Nanopart. Res. **4**, 499 (2002).
[30] K. Yatsui, T. Yukawa, C. Grigoriu, M.Hirai, W.Jiang, J. Nanopart. Res., **2**, 75, (2000).
[31] L. Lanvete, G. Ausanio, A. C. Barone, C. Hison, V. Ianotti, S. Amoruso, R. Bruzzesse, M. Vitiello, M. D. Incou, P. Scardi, J. Optoelectron. Adv. Mater. **8**(5), 1672 (2006).
[32] D. Bauerle, Laser Processing and Chemistry, Springer, Berlin (2000).

*Corresponding author: simac@ifin.nipne.ro